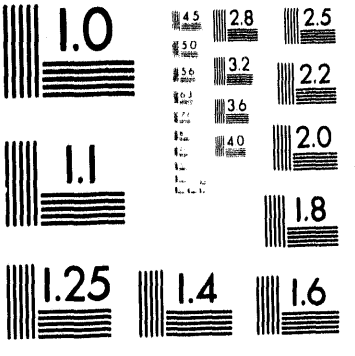
1.0
2.8
2.5
3.2
2.2
3.6
2.0
4.0
1.1
1.8
1.25
1.4
1.6

1 of 1

2

CONF-930516--6

Effects of Magnetic Field Perturbations in the ATF Torsatron*

R. J. Colchin, S. C. Aceto,** A. C. England, R. C. Isler, M. Murakami, D. A. Rasmussen, T. Uckan, J. B. Wilgen, and J. J. Zielinski**

Oak Ridge National Laboratory, Oak Ridge, Tennessee, 37831, USA

The effects of errors in the magnetic fields of tokamaks on the plasma are quite different from those in stellarators. In tokamaks, field errors can cause disruptive locked modes [1–3] through the non-linear evolution of tearing modes acting on initially small error-induced islands. Scaling predictions [3] for these effects indicate that the critical relative field error which can be tolerated becomes smaller as the tokamak size becomes larger. In stellarators, the effect is more benign, as field errors appear only to cause increased plasma transport in the vicinity of islands. Great care has been taken to minimize magnetic field errors in the most recent generation of stellarator-type magnetic plasma traps [4–7]. These efforts stem from the realization that relative field errors of order of $\Delta B / B \sim 10^{-3}$ (where the field error ΔB is applied in a toroidal field B) can form flux surface islands, leading to a more rapid loss of plasma.

In the past six years, several new and sensitive techniques have been developed to detect and map field errors [4, 7, 8–11]. These methods all rely on the detection of electrons injected along magnetic field lines. During the commissioning of ATF, flux surfaces were mapped using the fluorescent screen technique [4, 9]. Field errors were discovered and traced to uncompensated dipoles in the helical current feeds [4, 12]. Prior to elimination of these errors, plasma discharges indicated centrally peaked plasma profiles [13]. After correction of the uncompensated dipoles, flux surfaces were mapped a second time, and the island widths were found to be greatly reduced.

Field errors were then deliberately introduced using a set of perturbation coils that had been added to ATF, and electron-beam mapping of the flux surfaces showed that islands several centimeters in width could easily be created by these coils. After elimination of the error fields, the measured plasma temperature and density profiles were much broader. The field-perturbation coils were then used to produce magnetic field asymmetries, and the measured plasma profiles were again shown to narrow as a result of islands.

EXPERIMENTAL RESULTS

Magnetic dipole coils separated by 180° were positioned on top of ATF's shell structure . Each dipole was located 1.1 m above the magnetic axis and consisted of 40 turns. The maximum current available for the dipoles was 6 kA, $I_{error}/I_{helical}$ = 20% at B_{z0}= 1 T, or $\tilde{B}_{z0} / B_{\phi 0} \leq 1.4\%$. Plots of the expected islands are shown in Fig. 1 at the toroidal angle of the Thomson

* Research sponsored by the Office of Fusion Energy, U.S. Department of Energy, under contract DE-AC05-84OR21400 with Martin Marietta Energy Systems, Inc.

**Rensselear Polytechnic Institute, Troy NY 12181, USA

DISTRIBUTION OF THIS DOCUMENT IS UNLIMITED

scattering diagnostic. This plot shows that field lines beyond the $\iota = 1/2$ surface do not form closed flux surfaces.

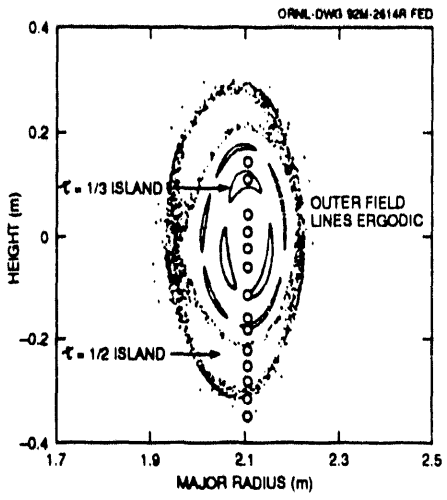

FIG. 1. Calculated flux surface islands formed when a perturbation of $\tilde{B}_z \cong 68\,G$ on axis is applied (6 kA in the perturbation coil for a 1 T helical field). The locations of Thomson scattering data points are shown as circles.

Plasma experiments were run with helical fields of 0.95 T on axis. The plasma was heated by 400 kW of 53 GHz microwave power.

A. Results without density control

Perturbing magnetic fields were introduced after stationary plasma conditions were established. Two types of experiments were performed: (1) the gas fueling was held constant; and (2) the line-averaged electron density was held constant by feedback control of the gas injection system. Measurements made without density control are discussed in this section.

The results of turning on the error field at 0.25 s after the beginning of the shot are shown in Fig. 2. The stored energy (as

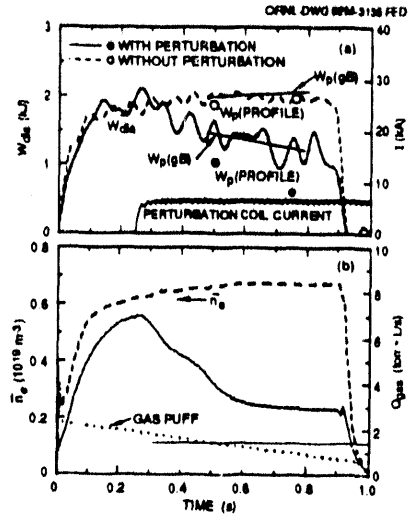

FIG. 2. (a) Diamagnetic stored energy as a function of time both with (solid line) and without (dashed line) a $\tilde{B}_z \cong 136\,G$ field perturbation after $t = 0.25$ s. Also shown are predictions of gyro-Bohm ($W_p(gB)$) scaling and the stored energy from Thomson scattering profile measurements. (b) The line-averaged density with and without the perturbation fields, and the gas puff flow rate. These measurements were made without feedback control of the gas puff.

measured by a diamagnetic loop) and the density decrease by a factor of two or more by the end of the discharge when compared to a discharge without applied perturbations. The density decay shown in Fig. 2(b) can be approximately characterized by two consecutive decay times of ~0.14 s: the first for the diffusion of the perturbing fields into the metal support structure, vacuum vessel and helical field coils, and the second for the subsequent field diffusion into the plasma. Figure 3 compares the electron temperature, density and pressure profiles for shots with and without magnetic field perturbations at 0.5 s (0.25 s after the fields were perturbed). Following the perturbation the density dropped, resulting in a central temperature rise due to the

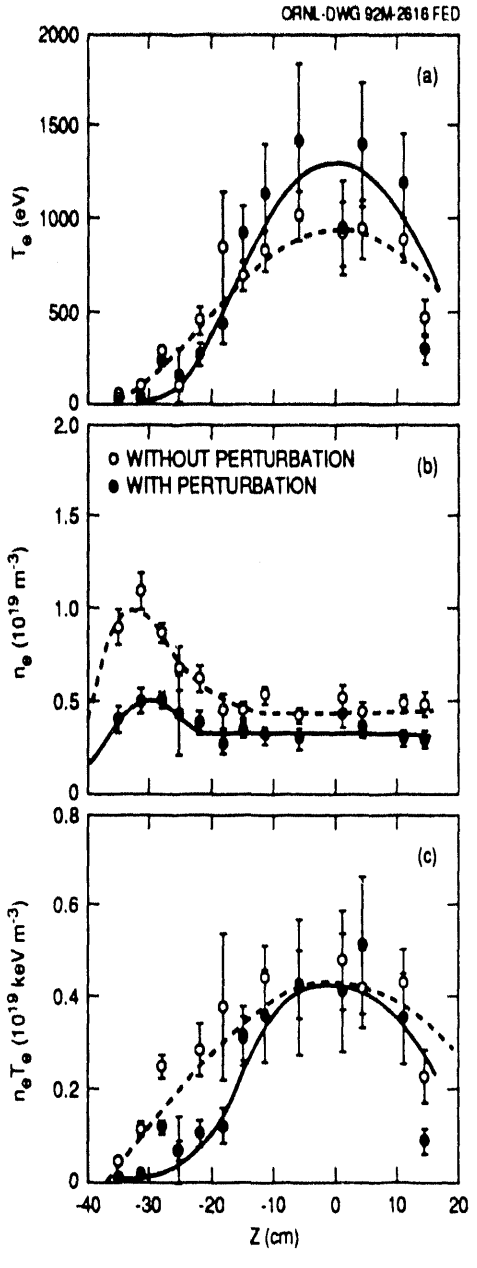

FIG. 3. Thomson scattering profile measurements of the temperature, density and pressure both with and without a $\tilde{B}_z \cong 136\,G$ perturbation. The measurements were taken at 0.5 s (0.25 s after the perturbation was initiated). There was no gas feedback control.

microwave power being applied to fewer electrons. Note that the pressure profile became more peaked after initiation of the perturbation. Fits to the data were constructed by a data-fitting routine that symmetrized the temperature and density profiles about the plasma axis. The geometry used in this symmetrization is based on the vacuum magnetic surfaces without magnetic field perturbations.

The plasma stored energy obtained from the Thomson scattering data of Fig. 3 is plotted at two points in Fig. 2(a) for both the perturbed and unperturbed cases and shows rough agreement with the diamagnetic signal. ATF experimental results [14, 15] have shown a strong

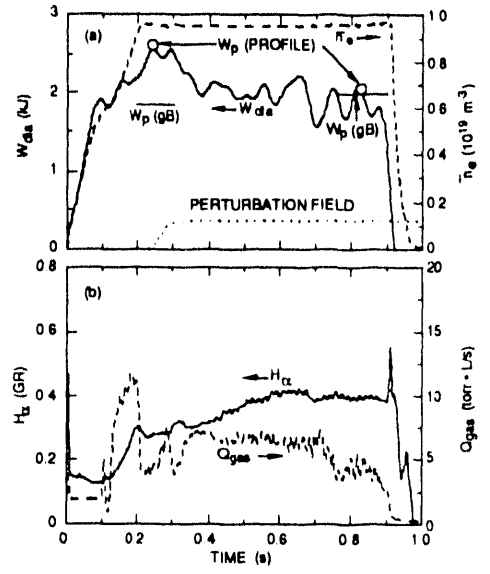

FIG. 4. (a) Diamagnetic stored energy as a function of time both with (solid line) and without (dashed line) a $\tilde{B}_z \cong 136\,G$ perturbation after t = 0.25 s. Also shown are predictions of gyro-Bohm ($W_p(gB)$) scaling and the stored energy from Thomson scattering profile measurements. (b) The H_α light emission measured at the wall and the gas puff flow rate. These measurements were made with feedback control of the gas puff, so that after an initial transient the density remained constant.

dependence of the confinement time on the density, as characterized by gyro-Bohm or Large Helical Device (LHD) scaling, i.e.

$\tau_E \sim n^{0.7}$. As shown in Fig. 3(a), the gross stored energy is within ±15% of the values predicted by gyro-Bohm scaling.

B. Results with density control

Figure 4(a) shows the stored energy and the density under conditions of density feedback control. The stored energy decreased by < 20% under these conditions, and the particle confinement time decreased by ~25% (i.e. an increase of ~25% in the H_α signal, Fig. 4(b)). Slightly higher density discharges have shown a doubling of the H_α signal with no decrease in the stored energy. The central ECE electron temperature decreased slightly, and the ion temperature was almost constant after plasma initiation.

The electron temperature, density and pressure profiles are shown in Fig. 5. The electron temperature profile was narrowed and the density profile was altered only in the outer region of the plasma. The pressure profile became narrower with the perturbation, as shown in Fig. 5(c). The stored energy calculated from profile measurements is compared with the diamagnetic measurement just before the perturbation and near the end of the discharge in Fig. 4(a), and shows reasonable agreement. The stored energy predicted by gyro-Bohm scaling is also shown.

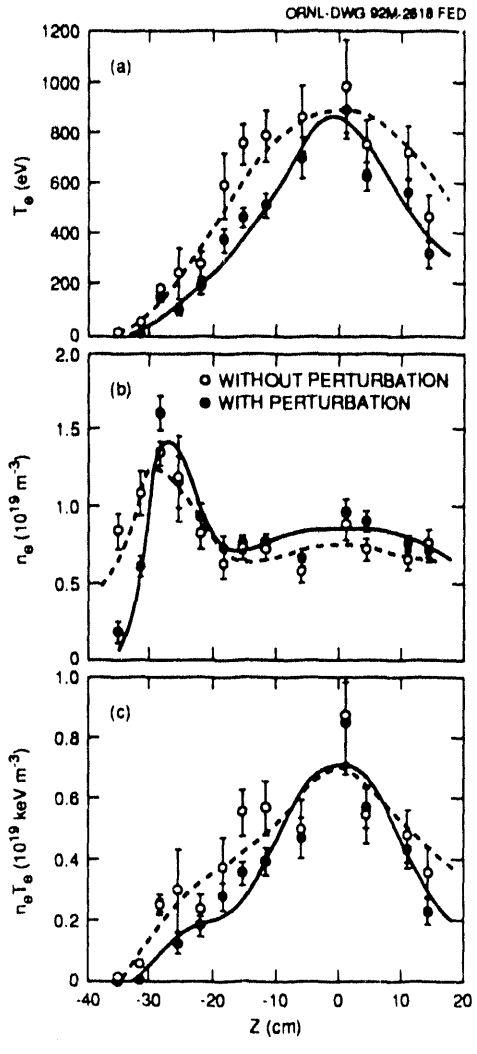

FIG. 5. Thomson scattering profile measurements of the temperature, density and pressure both with and without perturbation. The measurements were taken at 0.75 s (0.5 s after the perturbation was initiated). Feedback control of the gas was applied to keep the density constant.

COMPARISON WITH OTHER EXPERIMENTS

Profile data (Figs 3 and 5) show that the plasma pressure remained constant near the axis after application of the field perturbation. However, in the (outer) region of the large $\iota = 1/2$ island, the pressure profile was reduced. This is consistent with the prior observation that similar perturbations which were present in the original magnetic field coil system [4, 13] caused the plasma profiles to be peaked.

The energy confinement time τ_E is observed to be directly dependent upon the density and changed only slightly when the density was held constant by feedback control of the gas puff. When feedback

control was not applied, the density and the energy confinement time were almost halved.

Although there was almost no effect on the potential at the limiter, the potential measured by the HIBP in the outer part of the plasma increased (with density feedback control). This would be expected if electrons preferentially escaped from the plasma region.

Similar experiments have been carried out on the Compact Helical System (CHS) and Heliotron E torsatrons [16–18] and in the TU-Heliac [19] but with quite different results. The geometry of the coils in CHS was similar to that employed in the ATF experiment, but additional coils were located below the midplane in Heliotron E. In those experiments, feedback control of the density was not applied and no change in the stored energy was observed when the plasma was located at its normal position. The applied axial perturbing field was $\tilde{B} / B = (1–2) \times 10^{-3}$ in CHS and $\tilde{B} / B = 2 \times 10^{-2}$ in Heliotron E. The null results in CHS might be explained by the low perturbation fields applied (10–20 G). The perturbations applied in Heliotron E were more nearly like those applied in ATF (≤156 G in ATF versus 200 G in Heliotron E). However, Heliotron E has much larger shear than ATF.

When the plasma was shifted outward ~5 cm or more in CHS and Heliotron E, a strong decrease in the energy confinement time was observed. This decrease may result from the fact that shifting the plasma outward places it in a region of smaller shear, where the island size becomes larger [18].

SUMMARY

The pressure profile in ATF is narrowed if a perturbation field ($\Delta B/B \sim 10^{-2}$) is applied, and the particle confinement deteriorates substantially. The reduction in the energy confinement time is modest if the dependence of the global energy confinement time on the density is taken into account. The changes observed in the H_α emission (with gas feedback control) suggest that field perturbations provide an external independent control on the particle confinement time.

These experiments indicate that field perturbations also provide an external control of the pressure profile. The peaking of the pressure profile qualitatively supports the earlier conclusions concerning the profile peaking which gave rise to second stability in moderate $\langle\beta\rangle$ discharges. Although there is no direct evidence for islands, the flattening of the pressure profiles at the outside edge of the plasma in the vicinity of the large $\iota = 1/2$ calculated islands suggests their presence.

The substantial deterioration of plasma parameters observed in ATF during field perturbations contrasts with the much smaller effects observed in other stellarator experiments.

REFERENCES

[1] SCOVILLE, J.T., LAHAYE, R.L., KELLMAN, et al., Nucl. Fusion **31** (1991) 875.

[2] MORRIS, A.W., FITZPATRICK, R., HENDER, T.C., et al., in Controlled Fusion and Plasma Physics (Proc. 18th Europ. Conf. Berlin, 1991), Vol. 15C, Part II, European Physical Society (1991) 61.

[3] FITZPATRICK, R., HENDER, T.C., Phys. Fluids B **3** (1991) 644.

[4] COLCHIN, R.J., ANDERSON, F.S.B., ENGLAND, A.C., et al., Rev. Sci. Instrum. **60** (1989) 2680 and references cited therein.

[5] YAMADA, H., MATSUOKA, K., OKAMURA, S., IDA, K., NISHIMURA, K., Rev. Sci. Instrum. **61** (1990) 686.

[6] LYSNYAKOV, G.G., VOLKOV, E.D., GEORGIEVSKIJ, A.V., et al., Study of the magnetic field configuration of an $\ell = 3$ torsatron by the triode method and the luminescent rod method, submitted to Nucl. Fusion.

[7] JAENICKE, R., ASCASIBAR, E., GRIGULL, P., et al., Detailed investigation of the vacuum magnetic surfaces on the W7-AS stellarator, submitted to Nucl. Fusion.

[8] HARTWELL, G.L., GANDY, R.F., HENDERSON, M.A., et al., Rev. Sci. Instrum. **59** (1988) 460.

[9] TAKAHASHI, R., MATUURA, H., MIZUUCHI, T., et al., in Proc. 6th Int. Stellarator/Heliotron Workshop (Kyoto, 1986) Vol. 1, PPLK-006, Kyoto University, Kyoto, Japan (1986) 220.

[10] HAILER, H., MASSIG, J., SCHULER, F., SCHWÖRER, K., ZWICKER, H., in Controlled Fusion and Plasma Physics (Proc. 14th Europ. Conf. Madrid, 1987), Vol . 11D, Part 1, European Pnysical Society (1987) 423.

[11] TOU, T.Y., BLACKWELL, B.D., SHARP, L.E., Rev. Sci. Instrum. **62** (1991) 1149.

[12] HARRIS, J.H., JERNIGAN, T.C., ANDERSON, F.S.B., et al., Fusion Technol. **17** (1990) 51.

[13] HARRIS, J.H., ANABITARTE, E., BELL, G.L., et al., Phys. Fluids B **2** (1990) 1353.

[14] COLCHIN, R.J., MURAKAMI, M., ANABITARTE, E., et al., Phys. Fluids B **2** (1990) 1347.

[15] MURAKAMI, M., ACETO, S.C., ANABITARTE, E., et al., Phys. Fluids B **3** (1991) 2261.

[16] OKAMURA, S., PERANICH, L., MATSUOKA, K., et al., in Stellarators (Proc. 8th IAEA Tech. Committee Mtg. Kharkov, USSR, 1991), IAEA, Vienna (1991) Paper IV-P-5.

[17] SUDO, S., ZUSHI, H., KONDO, K., et al., Nucl. Fusion **31** (1991) 2349.

[18] PAVLICHENKO, O.S., Nucl. Fusion **32** (1992) 157.

[19] WATANABE, H., KITAJIMA, S., TAKAYAMA, M., ZAMA, T., in Stellarators (Proc. 8th Tech. Committee Mtg. Kharkov, 1991), IAEA, Vienna, (1991) Paper IV-P-6.

DISCLAIMER

This report was prepared as an account of work sponsored by an agency of the United States Government. Neither the United States Government nor any agency thereof, nor any of their employees, makes any warranty, express or implied, or assumes any legal liability or responsibility for the accuracy, completeness, or usefulness of any information, apparatus, product, or process disclosed, or represents that its use would not infringe privately owned rights. Reference herein to any specific commercial product, process, or service by trade name, trademark, manufacturer, or otherwise does not necessarily constitute or imply its endorsement, recommendation, or favoring by the United States Government or any agency thereof. The views and opinions of authors expressed herein do not necessarily state or reflect those of the United States Government or any agency thereof.

Effects of Magnetic Field Perturbations on ATF Plasmas†

R. J. Colchin, S. C. Aceto,*
A. C. England, R. C. Isler, M. Murakami,
D. A. Rasmussen, T. Uckan, J. B. Wilgen, and J. J. Zielinski*

Oak Ridge National Laboratory, USA

9th IAEA Workshop on Stellarators
May 10–14, 1993

Garching, Germany

* Rensselaer Polytechnic Institute, NY 1218, USA
† Nuclear Fusion, 33 (1993) 323

Introduction

- Comparison of Error Field Effects in Tokamaks and Stellarators
  - Tokamaks - Induce tearing modes which lead to locked modes and plasma disruption
    - Field error tolerance becomes smaller as the tokamak becomes larger
  - Stellarators - Island formation leads to enhanced diffusion

- Field Errors Minimized in Recent Stellarators
  - New field error detection techniques developed
  - $\Delta B / B_0 \leq 10^{-3}$

ATF Field Perturbations

- Electron Beam Field Mapping in ATF
  - Field errors initially detected due to current feeds
  - Field errors reduced by redesigned of current feeds
  - Field perturbation coils introduced, large islands mapped
- ATF Plasma Conditions
  - Initial field errors caused peaked T_e & n_e profiles
  - Removal of field errors caused T_e & n_e profiles to broaden
  - Perturbations coils caused T_e & n_e profiles to again become more peaked

ATF
Experimental Set Up

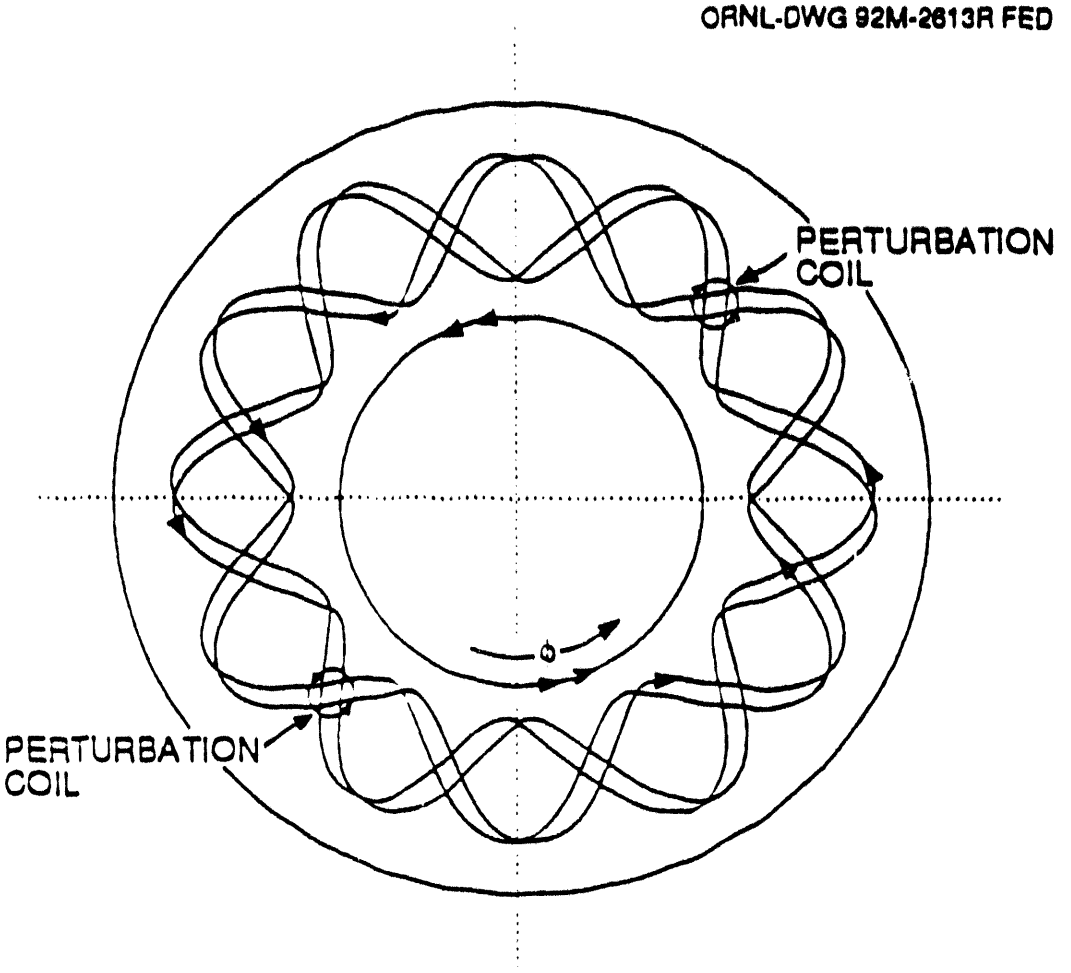

• Top View

Measured $\iota = 1/2$ Island Width

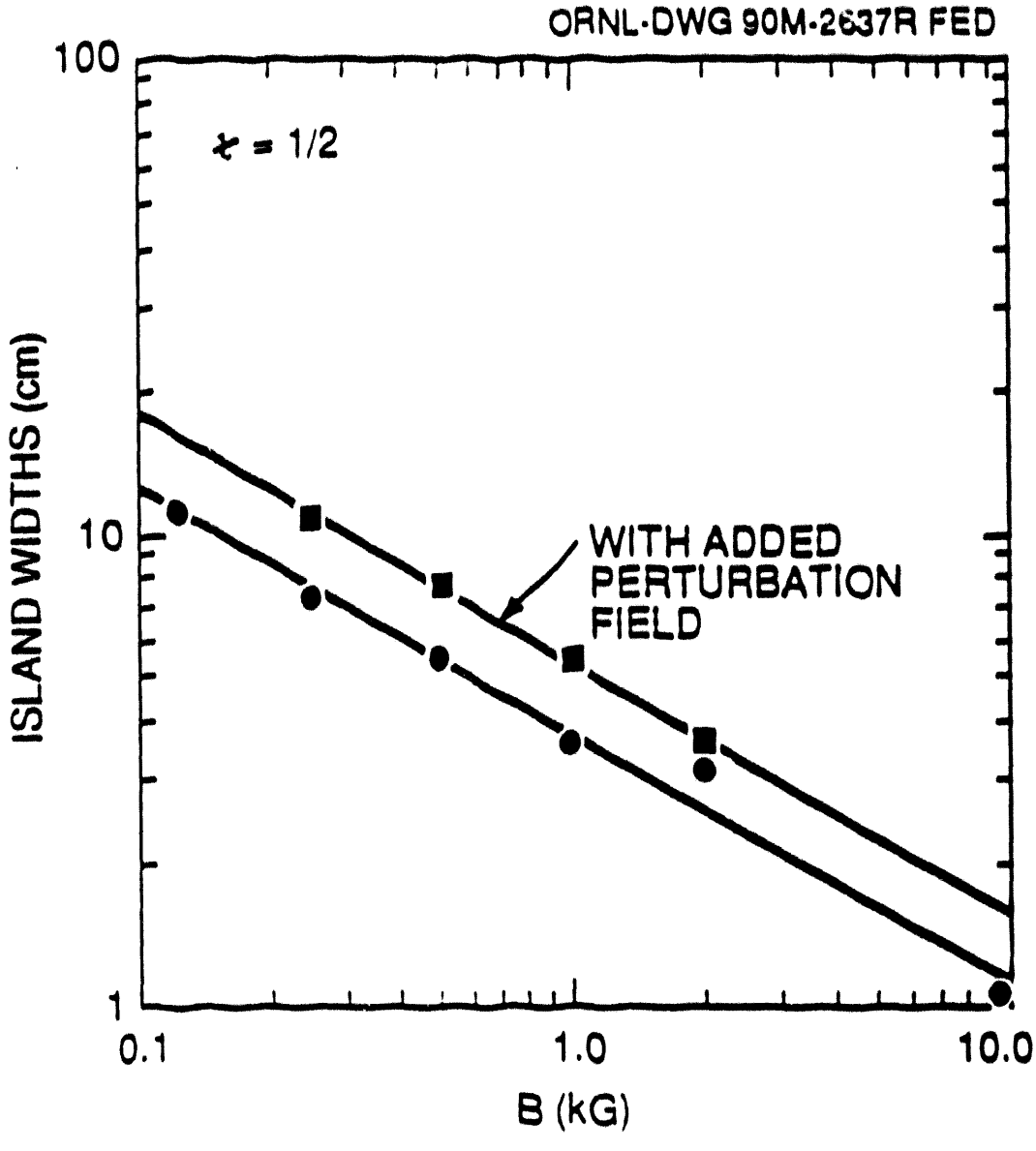

- Island Width ~ $B^{-1/2}$
- $I_{coil}/I_{helical} = 10\%$
- $\Delta B_{z0}/B_{\phi 0} \leq 0.7\%$

Measured $\iota = 1/3$ and $\iota = 2/5$ Island Widths

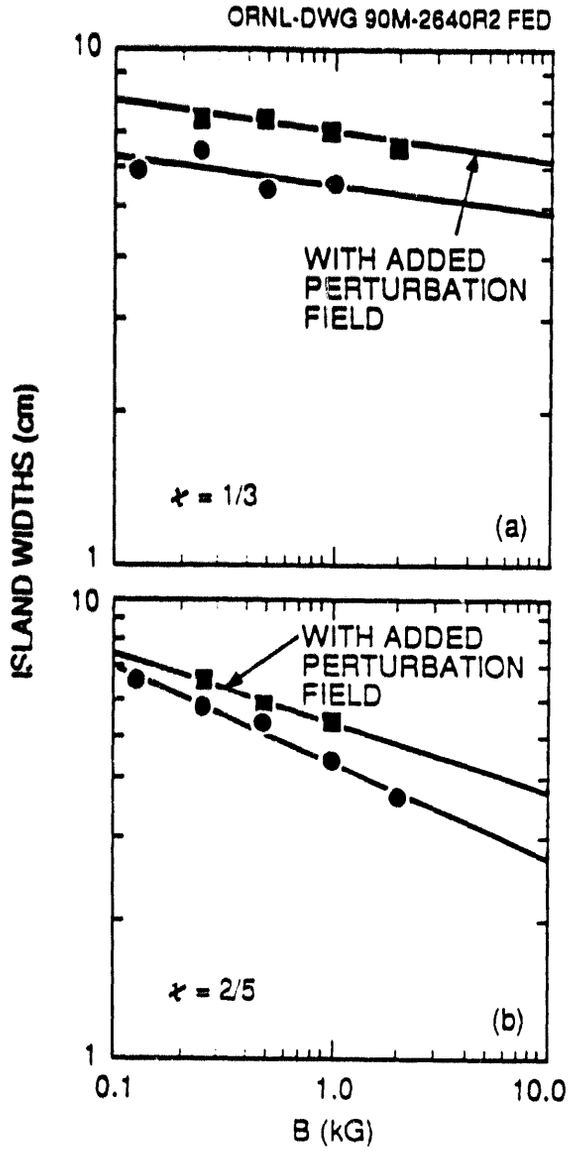

- Island Width $\neq B^{-1/2}$

Calculated Islands

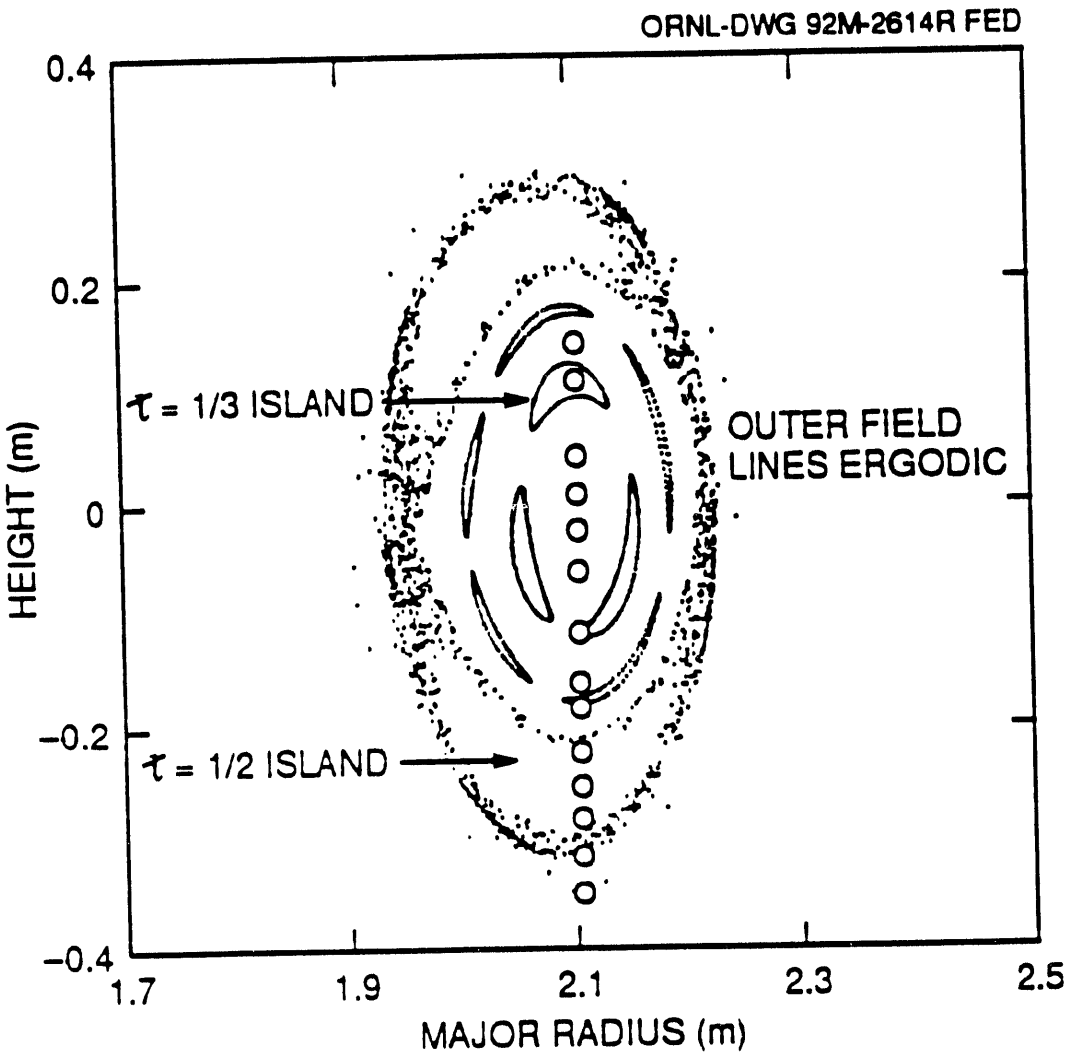

- $\Delta B_{z0} = 68$ Gauss
- $B_{\phi 0} = 9{,}800$ Gauss

T_e, n_e and Pressure Profiles Without Density Control

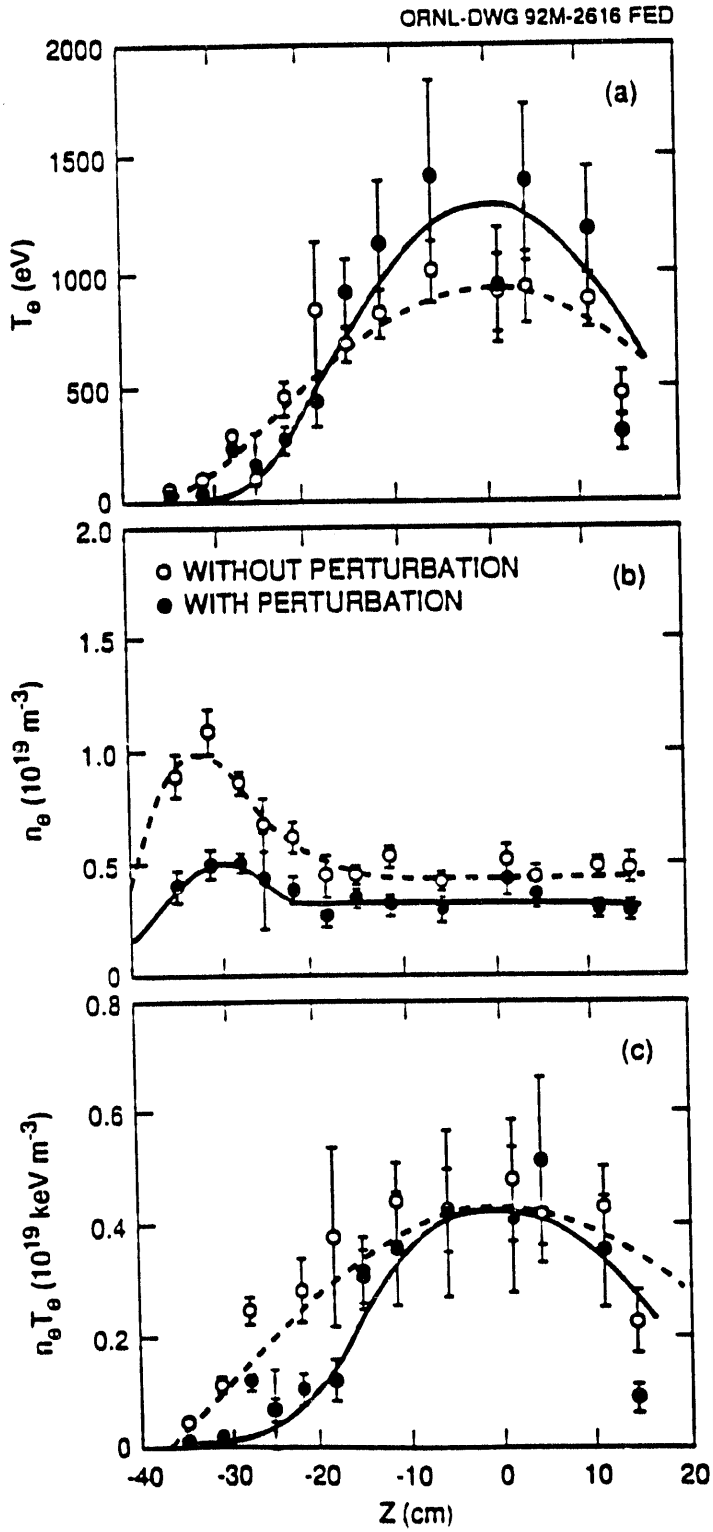

- Data Taken 0.25 s After Perturbation Turn On
- ΔB_{z0} = 136 Gauss

W_{dia} and $\bar{n}_e$ Without Density Control

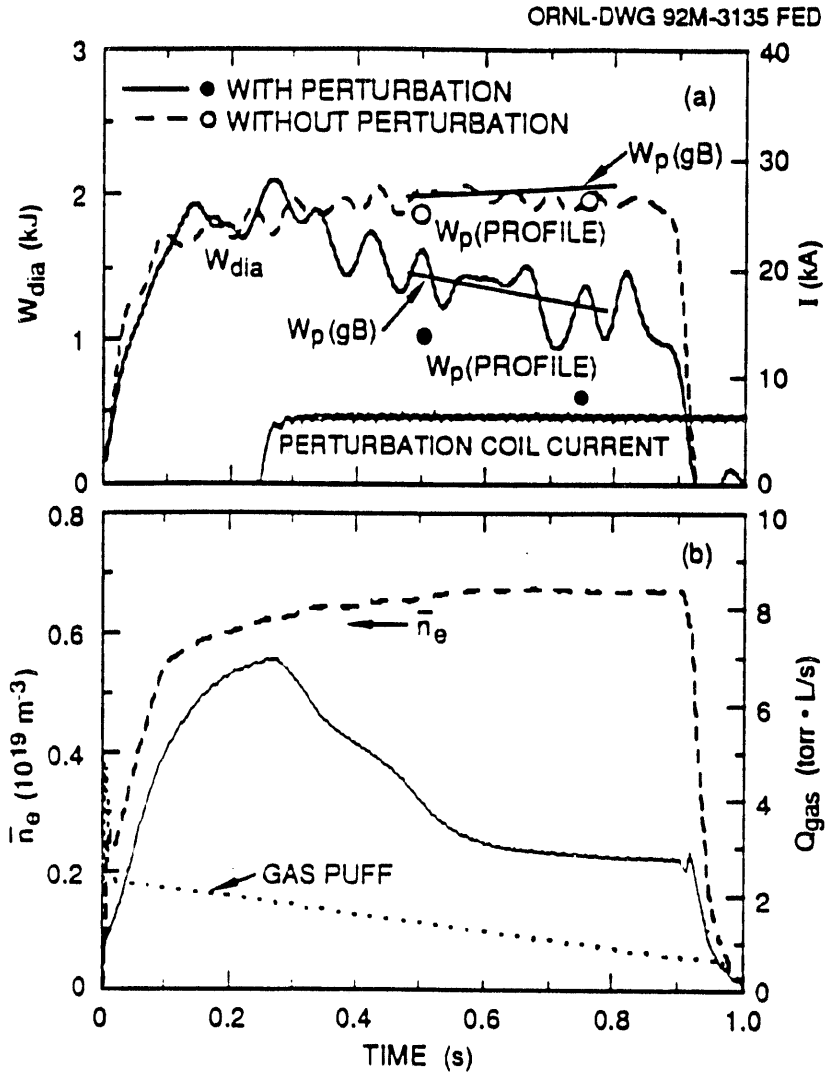

- W_p(Profile) = Thomson Scattering Data
- W_p(gB) = Gyro-Bohm Prediction
- ΔB_{z0} = 136 Gauss

T_e With and Without Density Control

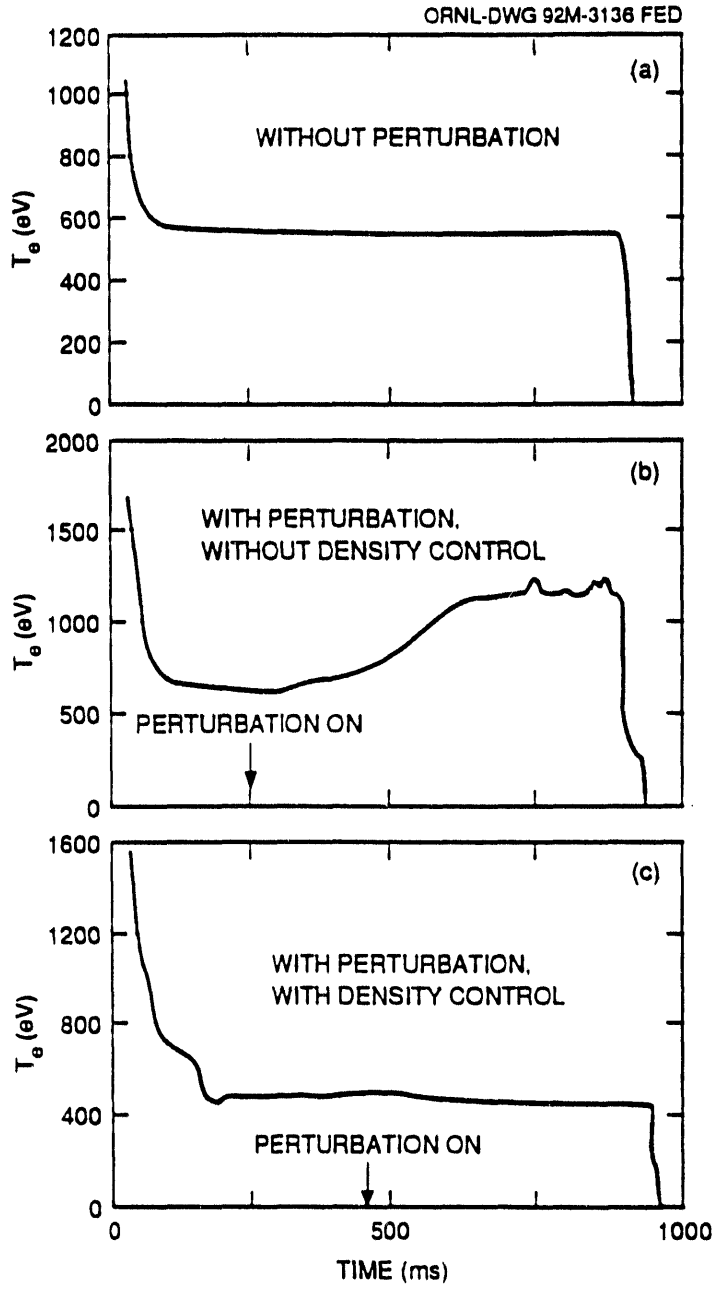

- **Without Gas Feedback Density Control, T_e Increases**

T_i With and Without Density Control

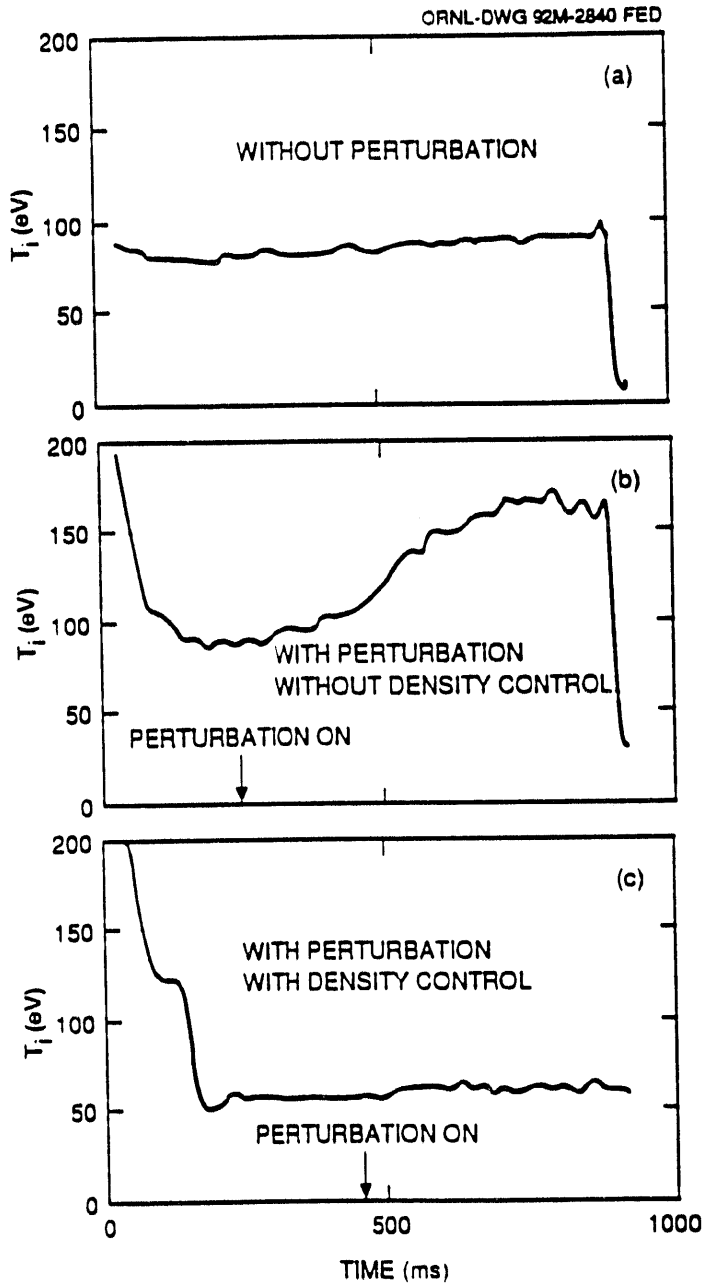

- T_i Follows the Same Pattern as T_e (C V measurement)

Fe XVI Emission With and Without Density Control

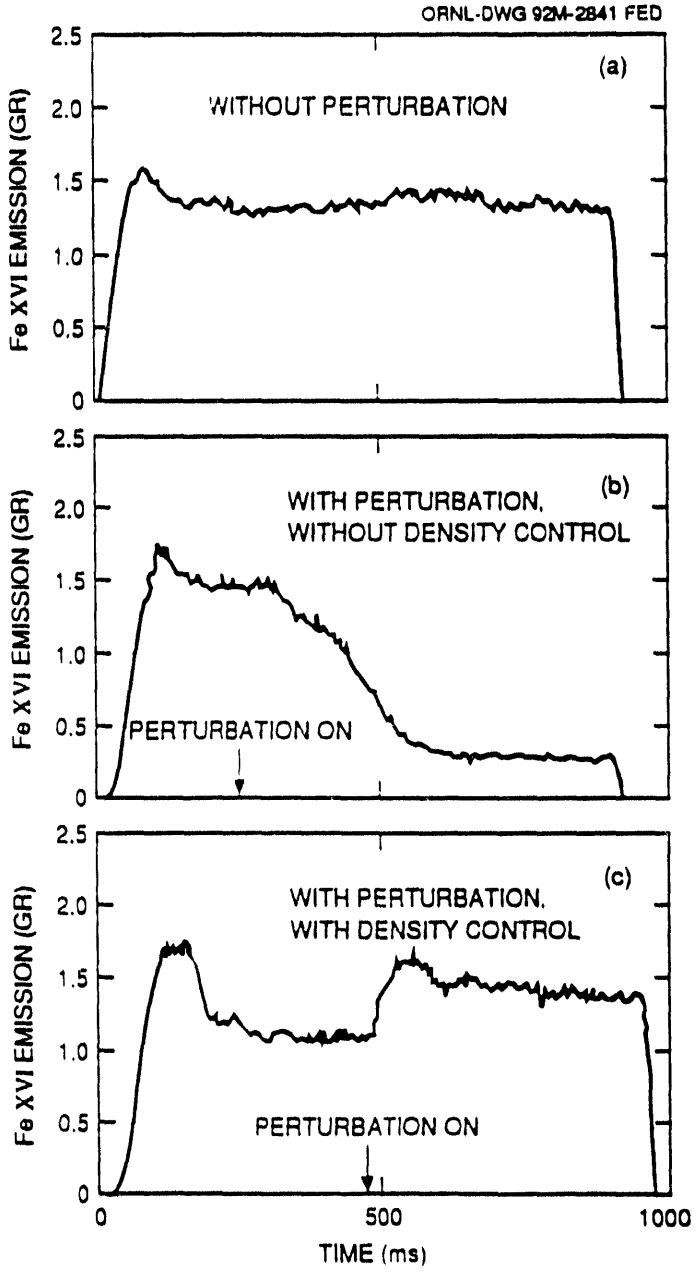

Fe XVI Emission With and Without Density Control

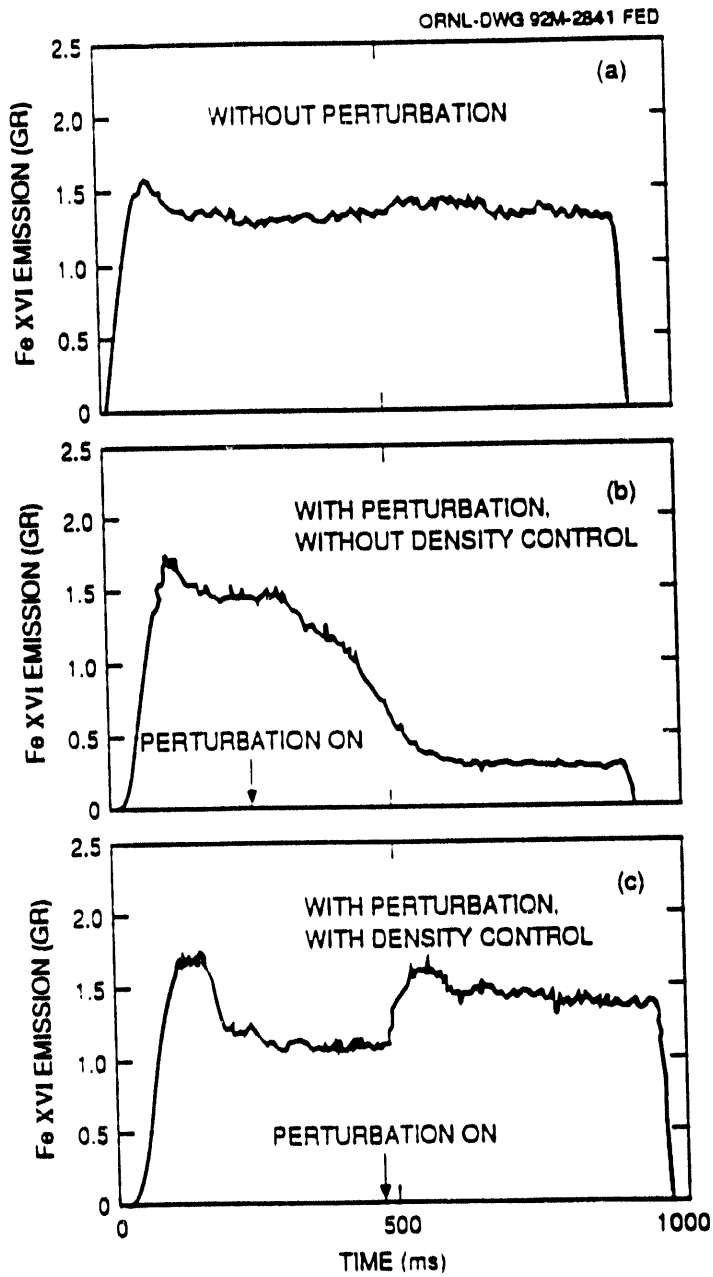

LANGMUIR PROBE DATA MEASURED AT THE LIMITER, a = 40 cm, AND H_α DATA MEASURED AT THE WALL WITHOUT DENSITY CONTROL

	Without Perturbation	With Perturbation
n_e (10^{19} m^{-3})	0.18	0.08
T_e (eV)	47	44
Φ_p (V)	94	108
H_α (GR)	0.22	0.34

T_e, n_e, and Pressure Profiles Without Density Control

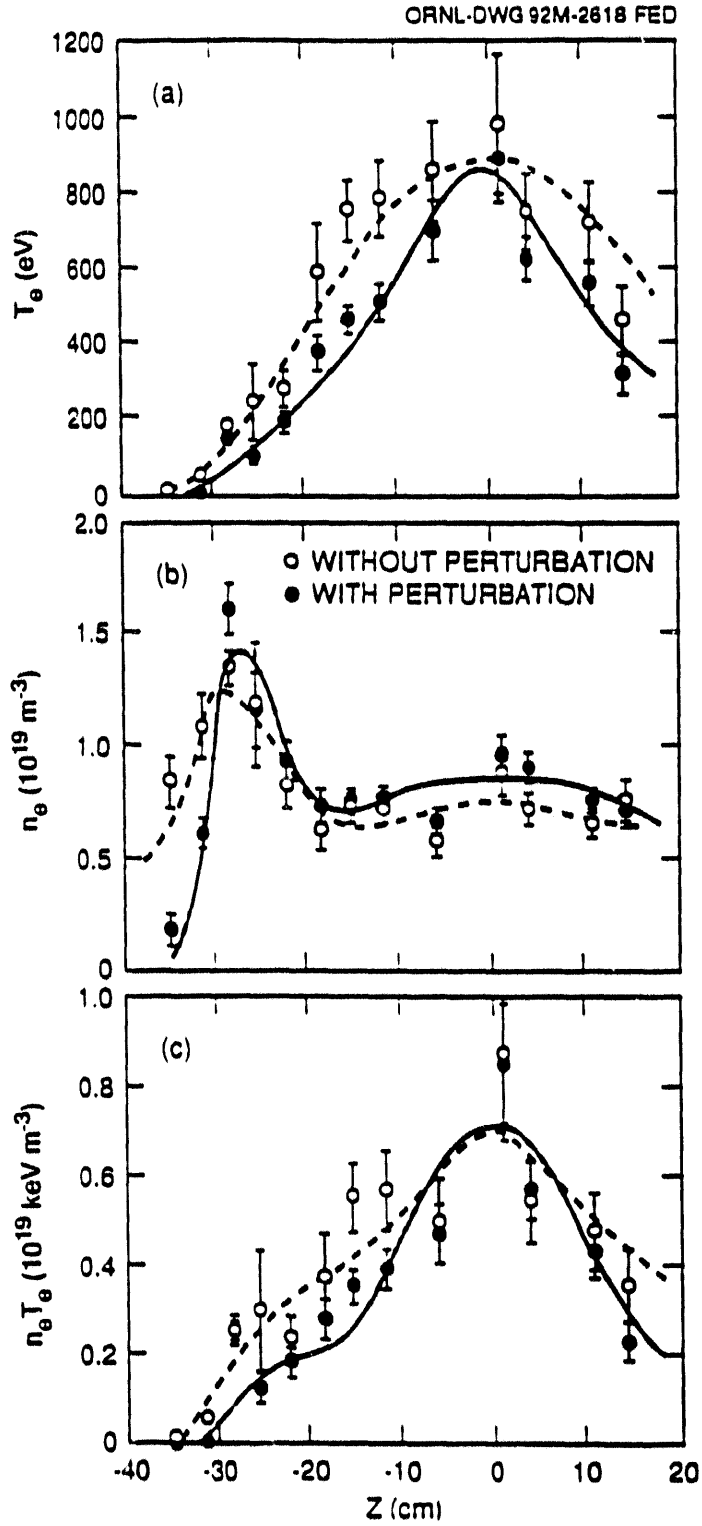

- **Data Taken 0.5 s After Perturbation Turn On**
- **ΔB_{z0} = 136 Gauss**

W_{dia}, $\bar{n}_e$, and T_e with Density Control

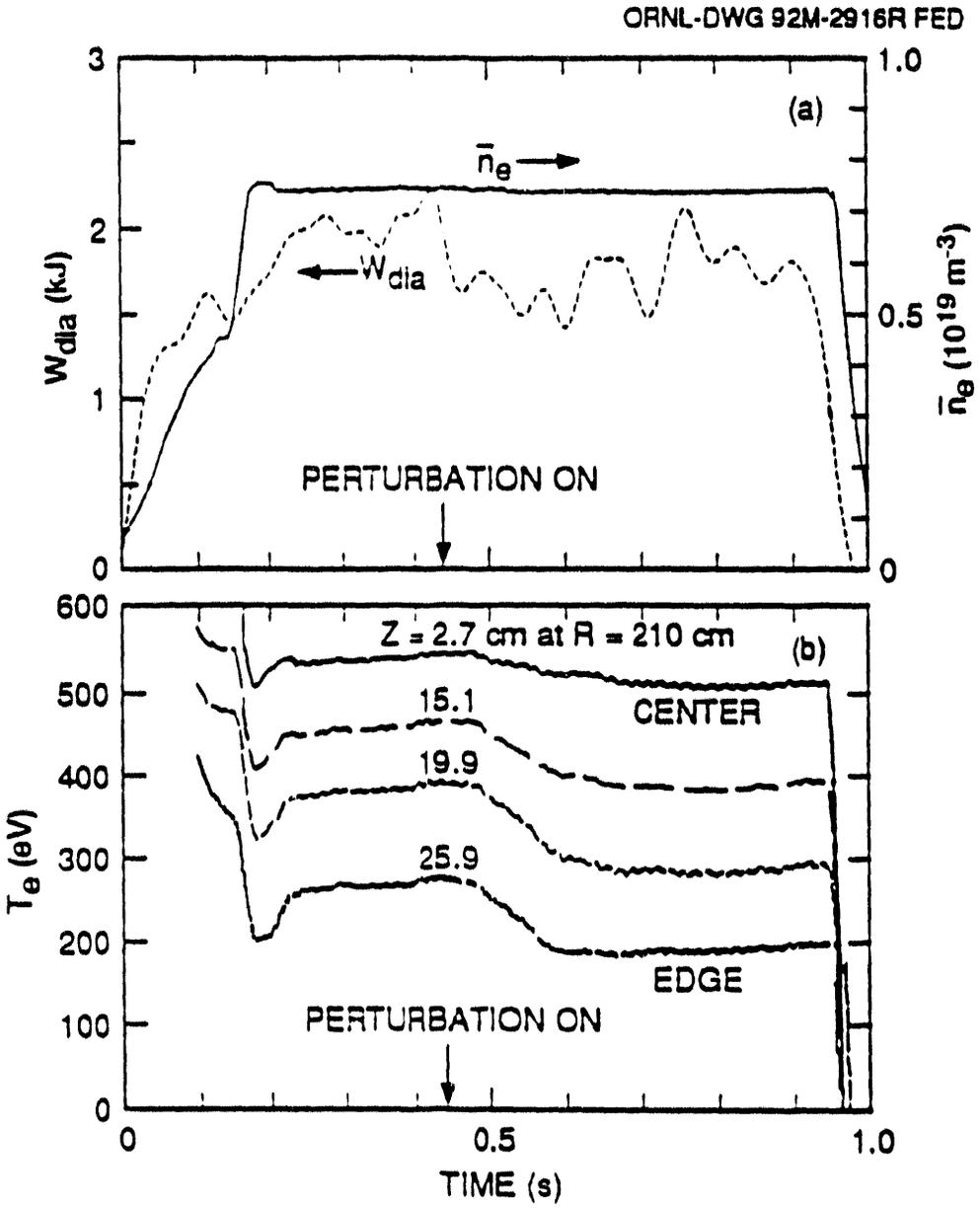

- **ECE Electron Temperature Data at Four Radii**

W_{dia}, $\bar{n}_e$, and H_α with Density Control

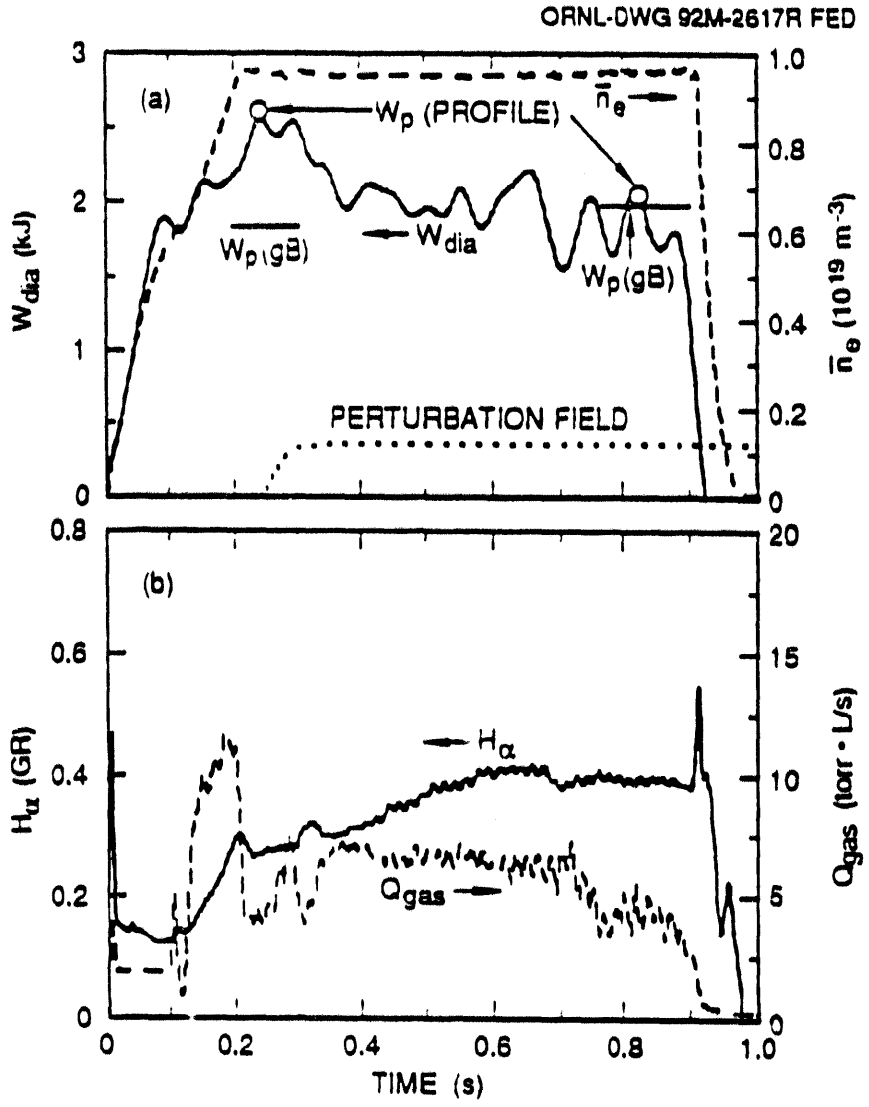

- W_p(Profile) = Thomson Scattering Data
- W_p(gB) = Gyro-Bohm Prediction
- ΔB_{z0} = 136 Gauss

Potential Profiles

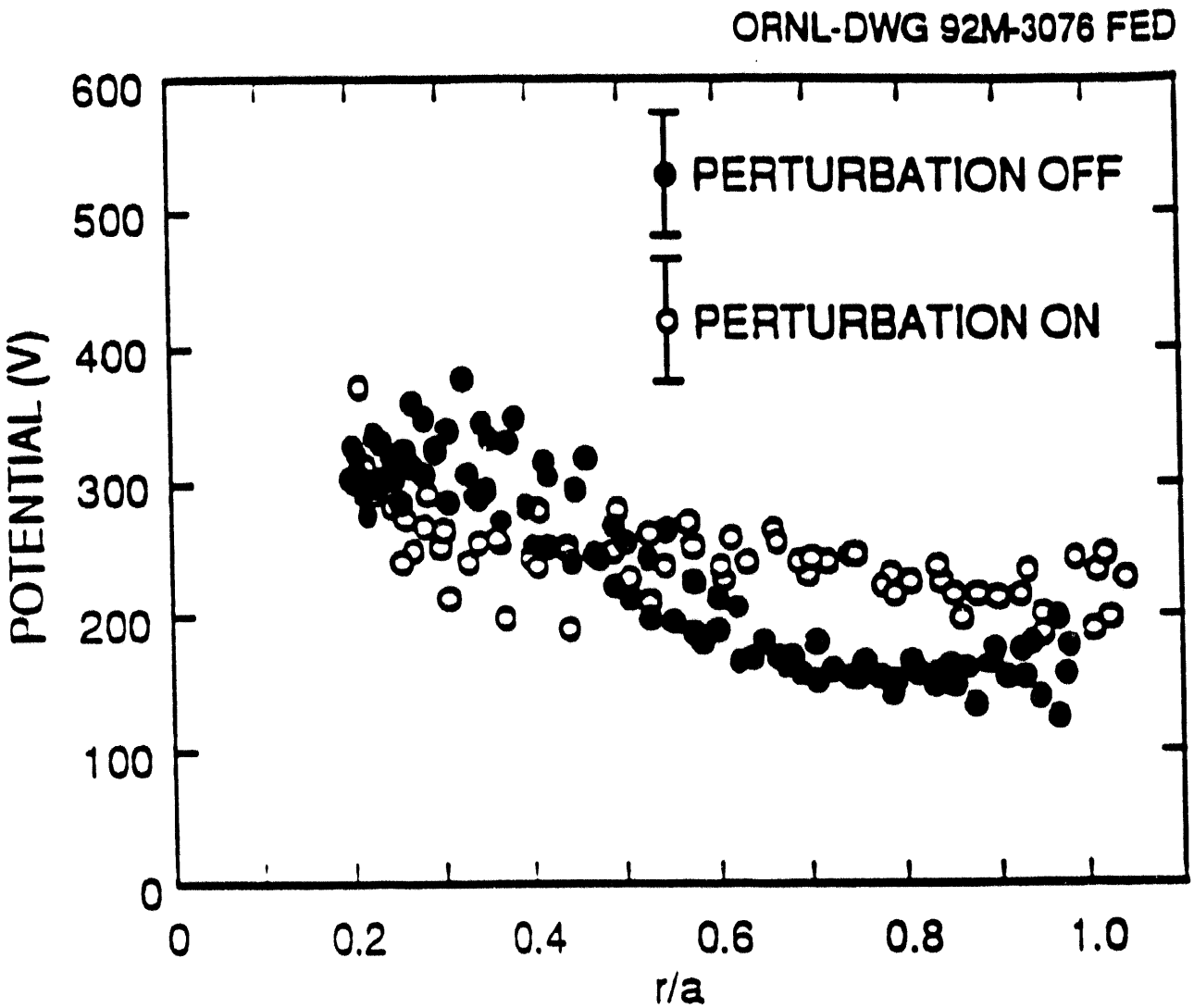

- **Profiles 0.33-.45 s After Perturbation Turn On**

H_α Light vs Time

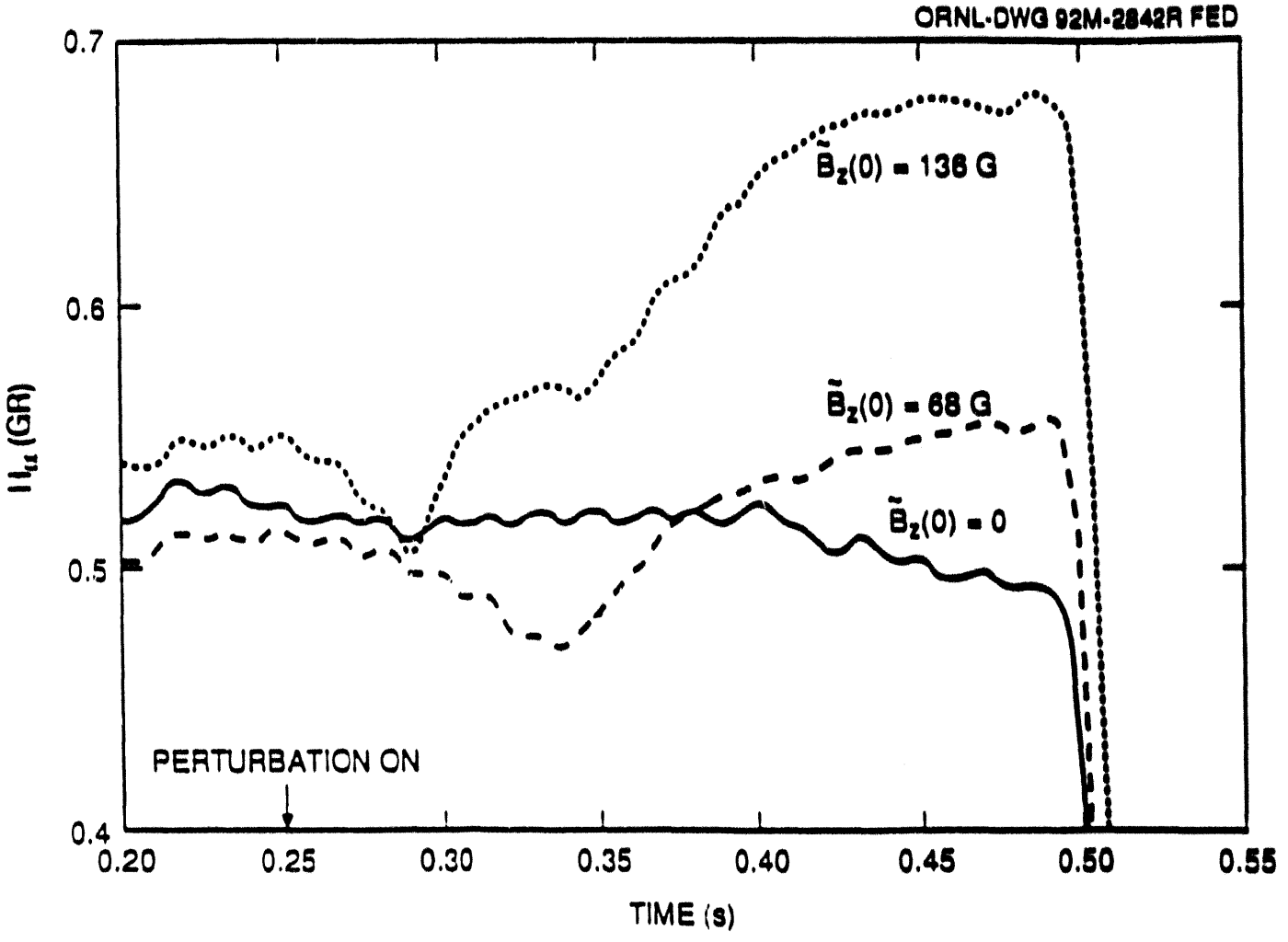

H_α Light vs Perturbation Strength

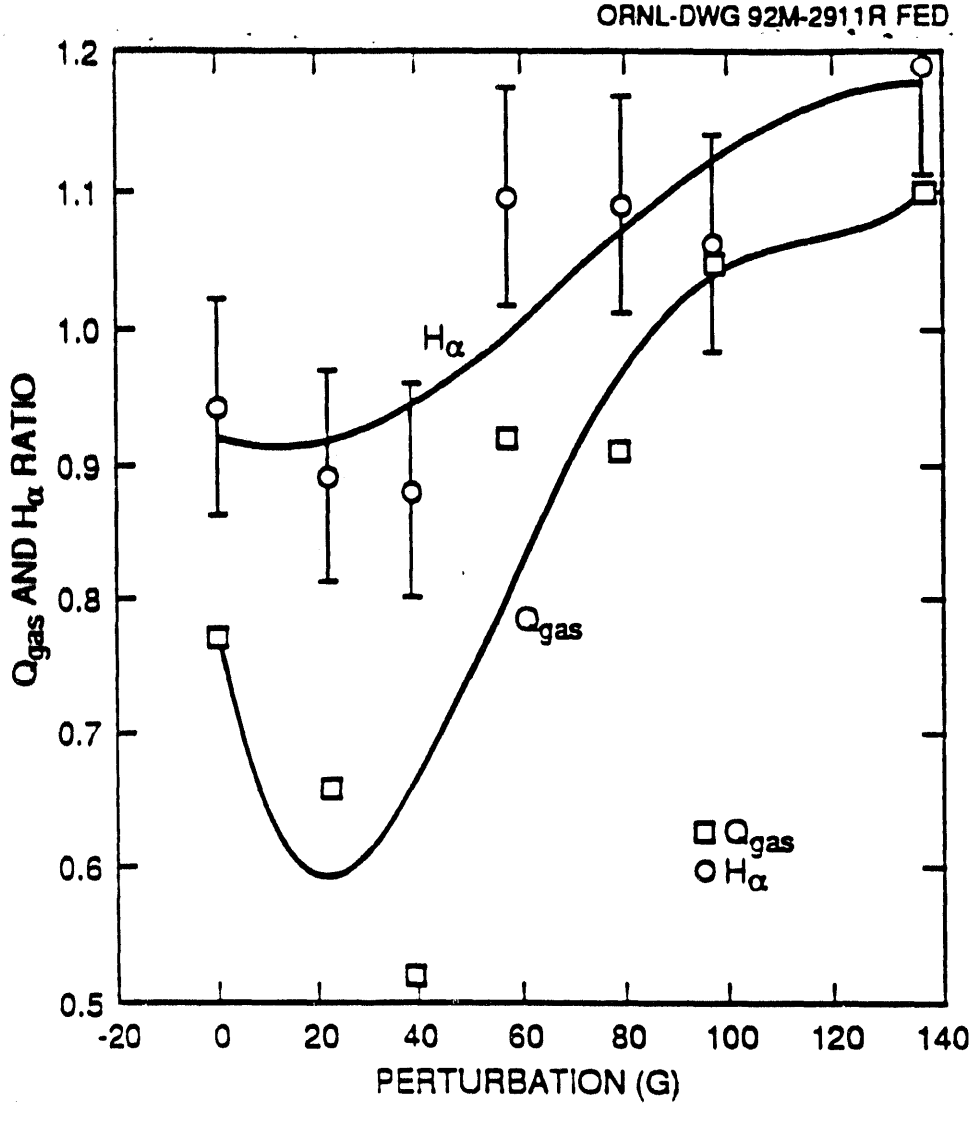

- **Data Ratio before Perturbation Turn On to Termination Time (t = 0.25 → t = 0.49 s)**

LANGMUIR PROBE DATA MEASURED AT THE LIMITER, $a = 40$ cm, AND H_α DATA MEASURED AT THE WALL WITH DENSITY CONTROL

	Without Perturbation	With Perturbation
n_e (10^{19} m^{-3})	0.55	0.55
T_e (eV)	38	36
Φ_p (V)	60	69
H_α (GR)	0.17	0.28

Summary

- Plasma Parameter Changes After Applied Perturbation ($\Delta B_{z0}/B_{\varphi 0} \approx 10^{-2}$).
    - Pressure Profiles are Narrowed in the Vicinity of the $\iota = 1/2$ island.
    - The particle confinement time decreases.
    - n_e and W_p are approximately halved (no feedback control of gas injection).
    - Gyro-Bohm confinement scaling remains valid.

- Magnetic Field Perturbations Provide an External Control on the Plasma Profile and Particle Confinement Time.

- Lesser effects observed in CHS and Heliotron-E without plasma shifts.

DATE
FILMED
12/6/93

END